

VISION SYSTEM FOR ON-LOOM FABRIC INSPECTION*

Hamed Sari-Sarraf and James S. Goddard, Jr.

Oak Ridge National Laboratory

Corresponding Author:

Hamed Sari-Sarraf, Ph.D.
Oak Ridge National Laboratory
Bethel Valley Road
Oak Ridge, Tennessee, 37831-6011
Phone: 423-574-5542
Fax: 423-574-6663
E-mail: sarisarrafh@ornl.gov

*Supported under the AMTEX Cooperative Research and Development Agreement at the Oak Ridge National Laboratory, managed by Lockheed Martin Energy Research Corporation for the U.S. Department of Energy under contract DE-AC05-96OR22464.

VISION SYSTEM FOR ON-LOOM FABRIC INSPECTION

Hamed Sari-Sarraf, *Member, IEEE*, and James S. Goddard Jr., *Member, IEEE*
Oak Ridge National Laboratory

Abstract-- This paper describes a vision-based fabric inspection system that accomplishes on-loom inspection of the fabric under construction with 100% coverage. The inspection system, which offers a scalable, open architecture, can be manufactured at relatively low cost using off-the-shelf components. While synchronized to the motion of the loom, the developed system first acquires very high-quality, vibration-free images of the fabric using either front or backlighting. Then the acquired images are subjected to a novel defect segmentation algorithm, which is based on the concepts of wavelet transform, image fusion, and the correlation dimension. The essence of this segmentation algorithm is the localization of those events (i.e., defects) in the input images that disrupt the global homogeneity of the background texture. The efficacy of this algorithm, as well as the overall inspection system, has been tested thoroughly under realistic conditions. The system was used to acquire and to analyze more than 3700 images of fabrics that were constructed with two different types of yarn. In each case, the performance of the system was evaluated as an operator introduced defects from 26 categories into the weaving process. The overall detection rate of the presented approach was found to be 89% with a localization accuracy of 0.2 in. (i.e., the minimum defect size) and a false alarm rate of 2.5%.

Index Terms-- Textile Industry, Fabric Inspection, Computer Vision, Real-Time Systems, Wavelet Transform, Defect Detection, Quality Assurance, Process Control

I. INTRODUCTION

Measurement of quality during the production of woven fabrics is highly important to the textile industry in lowering costs and improving the finished product. Presently, much of the fabric inspection is

performed manually by human inspectors and using off-line stations. Many defects are missed, and the inspection is inconsistent, with its outcome depending on the training and the skill level of the personnel. As a result, the textile industry has been moving toward automated fabric inspection. An automated fabric inspection system can provide consistent results that correlate with the quality-control standards of the textile industry. Up to this point, most if not all of such automated technologies have been off-line (or off-loom), inspecting large rolls of fabric after they have been produced. To provide the most precise control of quality, however, the fabric must be monitored as it is constructed so that corrections can be made immediately to minimize the quantity of poor-quality fabric. In addition, higher production speeds make the timely detection of defects more important than ever.

There are more than 50 identified categories of fabric (weaving) defects in the textile industry. It is interesting to note that approximately 80% of these defects have a preferred orientation, either in the direction of motion (i.e., warp direction) or perpendicular to it (i.e., pick direction). Many defects are caused by machine malfunctions, while others are due to faulty yarns. For air-jet looms, which are the most widely used, the predominant defects are misspicks (missing or broken pick yarns), end-outs (missing or broken warp yarns), and slubs (or waste). These looms, as well as other less widely used looms, may have machine faults that produce other defects, such as holes, oil spots, or dirt. These assorted defects can produce a wide range of visible effects on the finished fabric and render it off-quality. Warp or pick defects tend to be long and narrow, slubs can produce point defects, and moiré defects change the apparent texture of the weaving pattern.

Automation of fabric inspection has been a topic of considerable research. The inspection systems are predominantly optically based and primarily use either line-scan [1-3] or area [4] sensors for image

Research supported under the AMTEX Cooperative Research and Development Agreement at the Oak Ridge National Laboratory, managed by Lockheed Martin Energy Research Corporation for the U.S. Department of Energy under contract DE-AC05-96OR22464.

acquisition. Complete real-time systems have been developed that emphasize the high-performance image acquisition and computing hardware requirements for discrete defect detection and classification [5,6]. Also widely reported are the image analysis methodologies, including those based on textural models for defect detection [7,8], as well as neural or knowledge-based techniques for defect classification [9-11]. Real-time defect detection approaches using the wavelet transform and fuzzy inferencing have also been described in [4,12].

The fabric inspection system, which was developed by the authors in early 1995 and is presented here, differs from existing systems in two crucial ways. First, it is on-line or on-loom; and second, it is equipped with a novel defect segmentation technique, which has been thoroughly tested under realistic conditions and found to have a high detection rate, high accuracy, and a low rate of false alarms. The results of comparably extensive tests have yet to be reported for the competing systems or for segmentation algorithms. The defect segmentation technique reported in [12] is noteworthy, as it takes our idea of preprocessing the fabric images using the wavelet transform to the next logical step by suggesting an optimal derivation of the wavelet bases. However, where we use the wavelet transform only as a preprocessing tool, this approach uses it as the primary means for defect detection.

In what follows, we describe the proposed fabric inspection system in terms of its image acquisition subsystem and its defect segmentation algorithm. The results of an extensive test for evaluating the performance of this system have also been included.

II. FABRIC IMAGE ACQUISITION

On-loom fabric image acquisition presents several challenges to obtaining high-quality, high-resolution images. One of these challenges is the isolation of the mounting components from the considerable vibration that is produced during loom operation. Another is the irregular forward motion of the fabric among the loom rollers after it is woven. Still another is the challenge of designing an inspection system whose cost-effectiveness can justify its use on many, if not all, of the looms in a manufacturing mill.

As described in the following sections, each of these challenges has been addressed and met in

developing our on-loom image acquisition subsystem.

A. Hardware Description

The image acquisition subsystem is implemented with standard components on a low-cost personal computer. These components, shown in Fig. 1, consist of a 4096-element, line-scan camera, which is synchronized to the moving fabric by means of an incremental encoder; a source of illumination for backlighting the fabric; a DSP-based image acquisition and processing card with a single TI 320C40 chip; and a personal computer. The only custom-made component in this subsystem is the camera-encoder interface, which is used to extract the true forward movement of the fabric from the highly oscillatory motion of the loom and to enable accurate image-line triggering for the line-scan camera. These components are used to acquire high-resolution, vibration-free images of the fabric under construction and to store them on the on-board memory of the acquisition card. The software running on the DSP board controls the image acquisition process and accumulates a two-dimensional (2-D) image suitable for the ensuing analysis (i.e., defect segmentation).

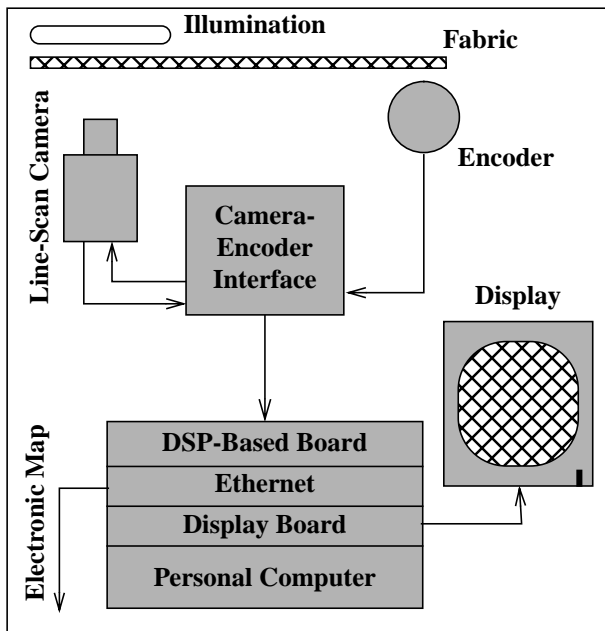


Fig. 1. The hardware components used in the inspection system.

B. Image Acquisition Operation

To extract the magnitudes and the frequencies of the physical displacements, vibration measurement and analysis were performed at potential mounting locations on a test loom. This analysis indicated that the most significant frequencies of interest were above 100 Hz. As a result, a mounting fixture was designed to attenuate the frequencies above this value.

To measure the true forward motion of the fabric, an optical incremental encoder was used. The actual encoder measurements indicated that the motion was quite irregular, but cyclical (see Fig. 2). Furthermore, the data showed that while the average motion of the fabric was in the forward direction, the fabric remained stationary during a portion of each cycle and, in some instances, even moved backward. To accurately characterize this pattern of motion, the camera-encoder interface monitors the encoder output and provides a digital response that corresponds to the true forward motion of the fabric. This circuit implements a state machine that remembers the backward motion signals. During operation, absent any backward motion, the state machine produces an output for every forward motion pulse from the encoder. If backward motion occurs, however, each backward pulse is counted, but no output is produced. With subsequent forward motion, the backward count is decremented at each forward pulse, again with no output. When the count reaches zero, the output is resumed for each forward pulse. The line-scan camera, which is synchronized to this forward output signal, produces a line of data when the fabric has moved forward by an amount corresponding to the prespecified inspection resolution.

During image acquisition, the camera exposure time is designed to be fixed, regardless of the loom speed. The fixed exposure time is realized by the exposure time control of the camera-encoder interface. A block diagram of the corresponding circuit is shown in Fig. 3. The encoder forward motion pulse presets a down counter to a value corresponding to the desired exposure time. This pulse also activates the pixel reset function on the camera, which clears any accumulated charge in the photosites. Thus the exposure time begins at this point. When the down counter reaches zero, the line transfer in the camera is activated and a line of image data is clocked out.

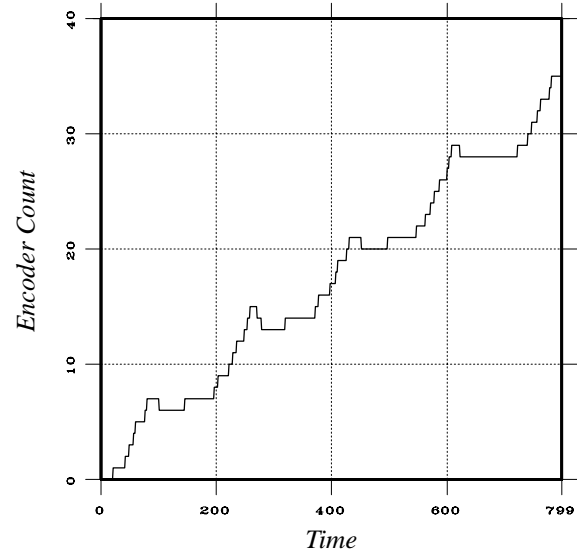


Fig. 2. Loom motion as measured by the encoder. The forward, backward, and even zero displacements of the fabric are all evident in this irregular yet cyclical pattern.

The exposure time is fixed as long as the time between the forward motion pulses is greater than the time it takes to clock the counter down to zero.

In general, backlighting the fabric has been found to produce higher-contrast images than those obtained by frontlighting. In this application, a fluorescent source, equipped with an aperture and driven by a high-frequency ballast, is used to backlight the fabric uniformly across its width. While the resolution of the acquired images in the pick (horizontal) direction is set by the optics of the camera, the resolution in the warp (vertical) direction is determined by the camera-encoder interface. The acquisition software, which initiates the start of an image frame, is used to specify such parameters as image width and height, integration time, and clock frequency.

Images that are generated using line-scan cameras are always degraded by linear artifacts that are oriented in the direction of motion. This degradation is due to the difference in responses of the individual sensor photosites. These artifacts are highly visible and can adversely affect the performance of the ensuing image analysis algorithms. A similar problem can occur with illumination and optics, where persistent nonuniformities give rise to noticeable artifacts in the generated images. To eliminate these effects,

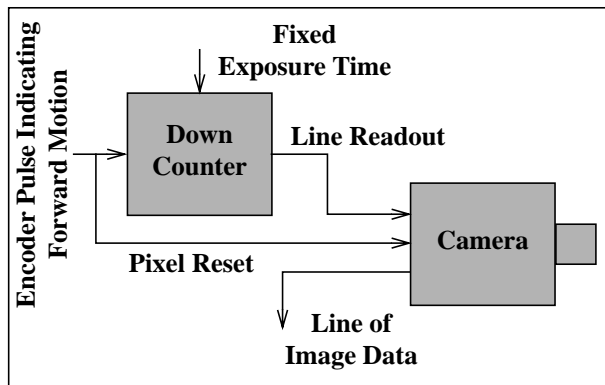


Fig. 3. Diagram showing how constant exposure time is achieved regardless of loom speed.

the preprocessing algorithm corrects for pixel and illumination nonuniformity. During setup, a white reference is obtained by first acquiring a large number of image lines (over 100) from the fluorescent source and with the fabric removed. Then these lines are averaged across their pixels to greatly reduce the noise that is due to the sensor and camera electronics. Finally, the inverse of each averaged pixel is calculated and the entire line is normalized to a maximum value of one. The resulting white reference is then used to correct for pixel and illumination nonuniformities by multiplying its values by the corresponding pixels of the acquired image lines.

The acquired image frame serves as an input to the image analysis or, more specifically, to the defect segmentation algorithm, which is also executed on the DSP board. To maintain full coverage of the fabric, the acquisition subsystem begins capturing the next frame while the current frame is analyzed for defects. The following section presents a detailed description of the defect segmentation algorithm.

III. DEFECT SEGMENTATION ALGORITHM

In designing the defect segmentation algorithm for our inspection system, we observed that the images of fabrics constitute ordered textures that are globally homogenous; that is, statistics measured from different patches in an image are correlated. It was further noted that images containing defects are less homogenous than those that are defect-free. Therefore, the essence of the presented segmentation algorithm is to localize those events (i.e., defects) in the image that

disrupt the global homogeneity of the background texture. We shall now describe the algorithmic modules (see Fig. 4) that are designed to accomplish this very goal under the conditions that

1. defects exhibit low-intensity variation within their boundary, and
2. relative to the textured background, they constitute a small portion of the field of view.

In the following sections, the modules are described in detail and their efficacy is clearly demonstrated using the images captured by the image acquisition subsystem.

A. Wavelet Transform Module

The wavelet transform module in the proposed segmentation algorithm constitutes a preprocessing step with the objectives of attenuating the background texture and accentuating the defects.

The term “wavelet transform” in fact refers to a specific class of the 2-D discrete wavelet transform called the multiscale wavelet representation (MSWAR) [13]. The notable advantages of MSWAR over the standard discrete wavelet transform, popu-

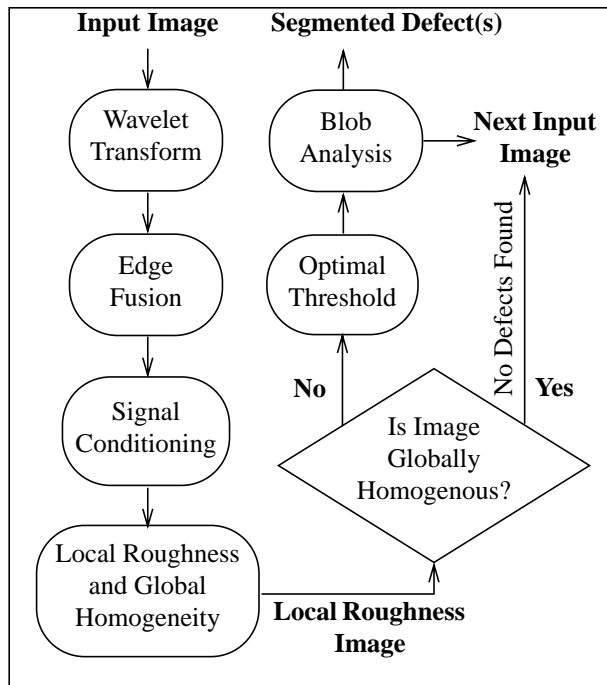


Fig. 4. Flowchart of the presented defect segmentation scheme, indicating its algorithmic modules.

larized by Mallet [14], are its shift invariance and the fact that in MSWAR, the transformed signals (or images) remain at full resolution with every iteration. These properties are especially important in anomaly detection and classification, because loss of resolution compromises the accuracy with which these tasks can be accomplished.

The MSWAR of a digital image $f(x, y)$, $(x, y) = 1, 2, \dots, N$, with M levels of scale reduction is a set of $(3M + 1)$ images. These are the detail images at all levels of scale reduction; that is, for $j = 1, 2, \dots, M$,

- $f_{d1}^j(x, y)$ (contains no vertical edges),
- $f_{d2}^j(x, y)$ (contains no horizontal edges),
- $f_{d3}^j(x, y)$ (contains no horizontal or vertical edges),

plus the blurred version of $f(x, y)$ at the lowest scale level, $f^M(x, y)$. An efficient algorithm for the generation of these images has been devised [13] and is given for easy reference.

1. Given a low-pass and a high-pass filter, and assuming that these filters are represented as column vectors LP and HP , respectively, generate four 2-D kernels as follows:

$$LP(LP)'^t, HP(LP)'^t, LP(HP)'^t, HP(HP)'^t,$$

where $(.)'^t$ represents vector transposition.

2. For $j = 1, 2, \dots, M$,
3. For $x = 0, 1, \dots, N - 1$,
4. For $y = 0, 1, \dots, N - 1$,
5. Allocate u row pointers, p_0, p_1, \dots, p_{u-1} , and u column pointers q_0, q_1, \dots, q_{u-1} , where u indicates the support of the selected filters.
6. Initialize the pointers as follows:

$$p_0 = x, p_1 = p_0 + 2^{j-1}, \dots,$$

$$p_{u-1} = p_{u-2} + 2^{j-1}, \text{ and}$$

$$q_0 = y, q_1 = q_0 + 2^{j-1}, \dots,$$

$$q_{u-1} = q_{u-2} + 2^{j-1}.$$

7. Convolve the generated kernels with the elements of the signal f^{j-1} , where $f^0 = f(x, y)$, as addressed by the pointers. The results are the $(x, y)^{th}$ elements of the four output signals f^j, f_{d1}^j, f_{d2}^j , and f_{d3}^j , respectively.

8. Next y .
9. Next x .

10. Next j .

An example of the application of this algorithm for the generation of MSWAR of a fabric image is shown in Fig. 5. Note that the objectives of texture attenuation and defect accentuation are clearly met in the top right-hand detail image in Fig. 5(c). The choice of the low-pass and high-pass filters is application-dependent. Thus far in this work, we have used Daubechies' D2 filter [15] because it is effortless and efficient to implement and, more importantly because the structure of its corresponding 2-D kernels matches the plain weave pattern of the fabrics under consideration. As reported in [12], other filters can also be derived in an optimal fashion to match the background textures of fabrics with other weave patterns.

Recall that the objectives of employing the MSWAR are to attenuate (in a scale-dependent fashion) the background texture and to accentuate the defects. The question is at what scale level and for which detail image these objectives are met. In other words, in Fig. 5, how can the image representing f_{d1}^2 , which seems to depict the defect clearly, be selected automatically for further processing? The appropriate choice of M is strongly dependent on the choice of the filters for MSWAR, as well as the resolution (i.e., number of pixels per unit area) of the captured images. Using this information, which is always available a priori, one should choose that value of M for which the greatest amount of background attenuation is achieved. Of course, care must be taken so that the defects remain intact during this smoothing process. Thus far, we have chosen to select an appropriate value for M manually by observing the output of MSWAR for a handful of fabric images.

Unlike the choice of M , the choice of the appropriate detail image depends on information that is seldom, if ever, available a priori (e.g., defect orientation). This is the reason for the use of the edge (detail image) fusion module, which is described in the following section.

B. Edge Fusion and Signal Conditioning

The main function of the edge fusion module is to complete the task that was initiated by MSWAR, that is, background attenuation and defect accentuation. Accordingly, this module is to produce an output,

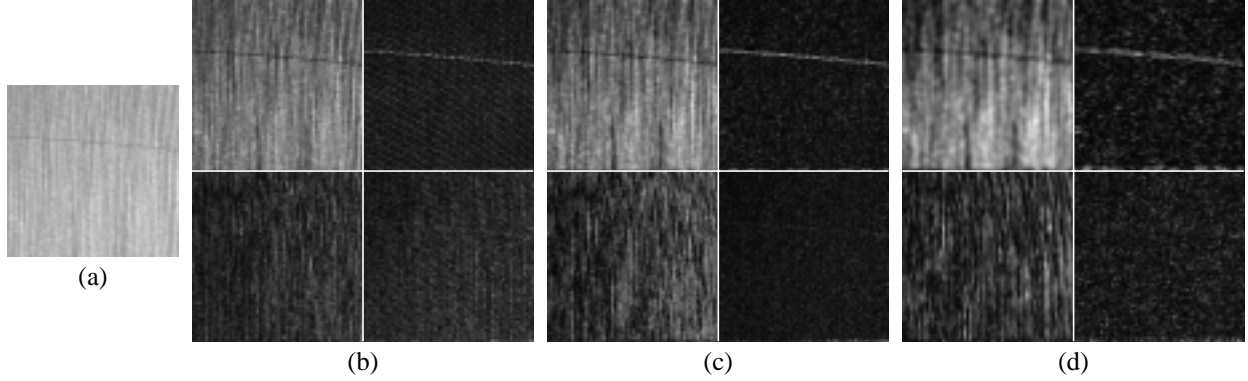


Fig. 5. (a) An image of a fabric with a pick defect (i.e., the dark, horizontal streak). (b), (c), (d) MSWAR of the image in (a) for $j = 1, 2, 3$, respectively. Starting with the top, left-hand corner and moving clockwise, the output images in (b), (c), and (d) correspond to f^j , f_{d1}^j , f_{d3}^j , and f_{d2}^j .

$o(x, y)$, in which for a preselected M , the pixels in the detail images that correspond to the defects are fully preserved. Although there are different approaches by which this task can be accomplished, we have chosen to use the following fusion scheme:

$$o(x, y) = \frac{\{f_1 + f_2 + f_3\} - \{[f_1 \times f_2] + [f_1 \times f_3] + [f_2 \times f_3]\}}{\{[f_1 \times f_2] + [f_1 \times f_3] + [f_2 \times f_3]\}}, \quad (1)$$

where multiplication is meant to be pixel-by-pixel and

$$f_i(x, y) = \frac{f_{di}^j(x, y) - \min[f_{di}^j(x, y)]}{\max[f_{di}^j(x, y)] - \min[f_{di}^j(x, y)]}, \quad (2)$$

for $i = 1, 2, 3$. Note that $f_i \in [0, 1]$ and that it is computed for a preselected value of M . To better understand the behavior of this fusion scheme, it is useful to examine it in a simpler form. This form, which is obtained by setting $f_3 = 0$ in Eq. 1, is known as Bernoulli's rule of combination and is often used in image fusion [16]. It is observed that in this form, for $f_2 = \text{constant}$, the mapping from f_1 to $o(x, y)$ is linear with $\text{slope} = 1 - \text{constant}$ and $y\text{-intercept} = \text{constant}$ (see Fig. 6). Note that the fused output tends to follow one of the inputs closely, if the other input possesses low values. On the other hand, the input with very high values tends to dominate the output, regardless of the value of the other input. This is precisely what is needed in our application, because in the detail images, defects -- interpreted as discontinuities in the textured background-- show up as pixels with high values.

An important issue that must be taken into account is that high values in the detail images represent not only the defects, but also the background texture. Therefore, unconstrained inclusion of all pixels (from all three detail images) in the fusion process will not, in most cases, result in background attenuation. To address this issue, we have constrained the fusion process as follows. Because the input image is assumed to be dominated by the background texture (rather than the defect), the energy (sum of squared values) for each of the detail images is computed and monitored. If, for a preselected M , one of the three detail images has an energy value that is disproportionately larger than the others [see f_{d2}^2 in Fig. 5(b)], but approximately equal to that of its counterpart, then that detail image is excluded from the fusion process. By its counterpart, we are referring to the corresponding detail image that has been computed from a reference image, that is, an image of the same fabric as the input image, but with no defects.

The next step in the presented defect segmentation algorithm is that of signal conditioning. The objective here is to make the defect pixels in the fused output more homogeneous. This objective is accomplished by the standard technique of histogram equalization [17], which, by increasing the global contrast of the image, compresses the dynamic range of the defect pixels. The importance of this step in the segmentation algorithm will become more apparent in the next section. An example of the application of these two modules to fabric images is presented at

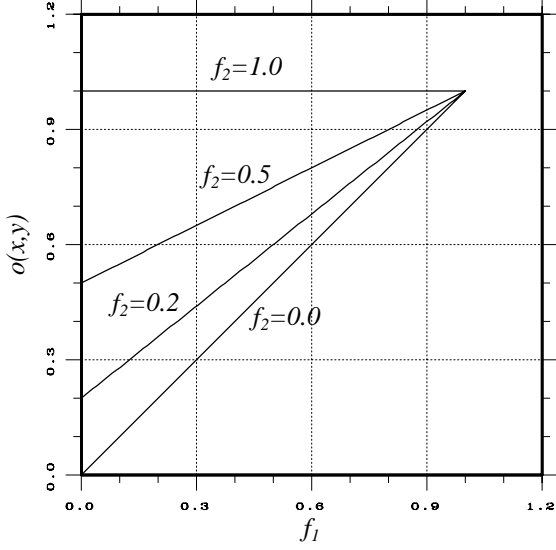


Fig. 6. Output of the fusion scheme when one of the two inputs is kept constant.

the end of the following section.

C. Global Homogeneity Module

As mentioned, in the proposed segmentation algorithm, defect segmentation is achieved by determining those events that disrupt the global homogeneity of the background texture. The local roughness and global homogeneity module constitutes the essence of the proposed approach.

Fractal-based measurements, such as the fractal dimension and the correlation dimension, have been utilized extensively for quantifying surface characteristics (e.g., surface roughness) of image textures. The proposed techniques for estimating the fractal dimension, however, are unreliable for localized measurements because they require adequately large data sets. In this work, two measurements, based on the correlation dimension, are used [18]. The first of these is a local measurement that quantifies the surface roughness; the second gives a measure of the surface homogeneity in a global sense.

Let a gray-level image, $f(x, y)$, be represented by a point in three-dimensional space as $\vec{X}_i[x, y, f(x, y)]$, $i = 1, 2, \dots, N^2$. The correlation dimension [19] is defined as where ϵ denotes scale. The correlation sum, $C(\epsilon)$, is given as where $\Theta(x)$ denotes the unit step function and

$$v = \lim_{\epsilon \rightarrow 0} \frac{\log[C(\epsilon)]}{\log[\epsilon]}, \quad (3)$$

$$C(\epsilon) = \lim_{N \rightarrow \infty} \frac{1}{N^2} \sum_{\substack{i, j = 1 \\ i \neq j}}^N \Theta(\epsilon - \|\vec{X}_i - \vec{X}_j\|), \quad (4)$$

$\|\vec{X}_i - \vec{X}_j\|$ is the distance between vectors \vec{X}_i and \vec{X}_j . Generally, the correlation dimension is estimated as the slope of the line that is fitted to the data points $\{\log(\epsilon), \log[C(\epsilon)]\}$. In this work, however, two measurements that are derived directly from the correlation sum are used.

The first of these reflects the local roughness of the input image surface and is given as

$$R(m, n) = \sum_{\epsilon=1}^{\epsilon_u} C^2(\epsilon, m, n), \quad (5)$$

where ϵ_u is the upper limit for ϵ , and $C(\epsilon, m, n)$ is the correlation sum computed within nonoverlapping subregions of the input image. The second measurement quantifies global image homogeneity and is computed as

$$V = \frac{1}{Q} \sum_m \sum_n [R(m, n) - M]^2, \quad (6)$$

where

$$M = \frac{1}{Q} \sum_m \sum_n R(m, n), \quad (7)$$

and Q is the total number of subregions into which the image is divided. Given these expressions, the following statements can be made. High values of $R(m, n)$ signify high correlation among the pixel values in the subregion (indicating a smooth surface), while low values of $R(m, n)$ indicate a rough surface. Furthermore, small values of V (i.e., surface is either mainly rough or mainly smooth) denote a globally homogeneous image.

By applying the local roughness and global homogeneity measures to the output of MSWAR (specifically, the fused detail images), one can robustly detect and localize anomalies in the presence of texture. To illustrate this point, consider the images in Fig. 7. The input images in Figs. 7(a) and 7(b) are of the same fabric, but the latter image contains a pick

defect (i.e., the dark, horizontal streak). The fused detail images are shown in Figs. 7(c) and 7(d), respectively. Comparing this pair of images with the input pair demonstrates the utility of the previously described preprocessing modules, that is, scale-dependent attenuation of the background texture and accentuation of the defect. Figures 7(e) and 7(f) depict the conditioned outputs, and the images in Figs. 7(g) and 7(h) represent $R(m, n)$ for each of the inputs. Note that on the one hand, the local roughness measure for the fabric with no defects exhibits a random pattern [Fig. 7(g)], while on the other hand, the same measure localizes the defect as an event with highly correlated pixels [Fig. 7(h)]. Furthermore, a comparison of the global homogeneity measures for the two fabrics (i.e., $V=58.1$ for the fabric with the defect versus $V=1.1$ for the one without) gives a clear indication of the presence of the defect. The significant, often an order of magnitude, difference between the values of V indicates that a threshold, T , can be established to robustly detect the presence or absence of defects. This threshold value is selected empirically by observing typical values of V for defect-free fabrics.

D. Thresholding and Blob Analysis

If the computed global homogeneity measure happens to fall below T , the input image is deemed to be defect-free, and the defect segmentation scheme begins to analyze the next acquired image frame. If, however, one or more defects are detected (i.e., $V > T$), the corresponding $R(m, n)$ is binarized by employing an automatic thresholding technique. The choice of a thresholding technique is not at all crucial, because large V 's indicate not only the presence of defects, but also the fact that the values corresponding to defects are vastly different from those corresponding to background. So far in this work, we have employed Otsu's approach [20], which aims to minimize the weighted sum of group variances. Although this approach has produced favorable results, we recommend that other techniques be explored in which the discrepancy between the number of defect pixels and the number of background pixels is taken into account, for example, [21].

Following the binarization of $R(m, n)$, the output image undergoes blob (connected component) analysis. For this, we have used one of the many widely

available blob analysis techniques, specifically, the two-pass technique presented in [17]. Once the blob analysis step is complete, the segmented defects can be categorized into a number of meaningful classes based on a few extracted features or attributes, such as size, orientation, and intensity profile.

IV. RESULTS

The performance of a prototype of the described inspection system was evaluated in two stages using a production-grade loom. In the first stage, the loom was set up to produce sheeting fabric using filament yarn with a plain weave pattern and pick and warp densities of 58 yarns/in. In the second stage of testing, the same construction was used, but this time with spun yarn. The prototype system was set up to cover a 20-in.-wide area of the fabric, with the understanding that, because of its scalability, one only needed to duplicate the system hardware to cover the full width of the loom. The loom was operated at the speed of 12 in./min as an operator introduced defects into the weaving process. The 17 defect types for the filament-yarn fabric and the 26 defect types for the spun-yarn fabric included almost all of the most commonly occurring weaving defects, such as mispicks, end-out, waste, kinky filling, oil, start mark, reed mark, mixed filling, moiré, dirty yarn, misreed, and hanging end.

The image acquisition subsystem consistently produced high-quality images of the fabric for both yarn types. Both the pick- and warp-direction image resolutions were set at 100 pixels/in. for the filament yarn and 200 pixels/in. for the spun yarn. The higher resolution in the latter case was necessary because the impurities that are naturally present in spun-yarn fabric tend to obscure the more subtle defects. The fixed exposure time of the line-scan camera was set at 2 msec. Note that with a nominal loom speed of 12 in./min and a maximum resolution of 200 lines/in., this exposure time is less than the shortest time between forward motion pulses (i.e., 25 msec) and therefore is sufficient to freeze the motion of the fabric. The performance of the image acquisition subsystem was evaluated as three observers determined whether or not the introduced defects were visually apparent in the captured images. Their judgement was that 91% of the defects in the filament-yarn fabric and 90% of the defects in the spun-yarn fabric

were “seen” by the prototype system.

The segmentation algorithm was invoked once a 2000×512 image frame was collected in the memory of the DSP board. To account for illumination nonuniformities, however, each frame was divided into sixteen 256×256 subimages before analysis. During the analysis of these subimages, the acquisition subsystem was directed to capture the next 2000×512 image frame so that 100% coverage of the fabric was maintained. The free parameters for the segmentation algorithm were set as follows. The level of scale reduction, M , was set to 2 and 3 for the filament- and the spun-yarn fabrics, respectively. This setting was prompted by the fact that the images in these cases, were captured at two different resolutions (i.e., 100 and 200 pixels/in.). The image subregion size for computing the local roughness was chosen to be 16, because defects less than 0.25 in. (i.e., 25 pixels) were deemed unimportant. Other parameters, such as V and the energy threshold for the constrained fusion process, were determined empirically.

In analyzing more than 3700 subimages for both fabric types, the overall detection rate of the pre-

sented approach was found to be 89% with a localization accuracy of 0.2 in. and a false alarm rate of 2.5%. The false alarm rate was computed as the total number of false detections divided by the total number of processed images. Note that the detection rate of 89% represents an average over all defect types. In general, because we are dealing with an edge-based segmentation approach, defects that produce very subtle intensity transitions (e.g., mixed filling, and moiré) were detected at a lower rate (i.e., 50-60%). On the other hand, for the most commonly occurring and the most serious defects, such as mispicks, end-outs, and slubs, the detection rate was 100% (see Fig. 8 for examples).

V. CONCLUSIONS

We have described a vision-based fabric inspection system that accomplishes on-loom inspection of the fabric with 100% coverage. The inspection system is scalable and can be manufactured at relatively low cost using off-the-shelf components. This system differs from those reported in the literature in two crucial ways. First, it is on-loom; and second, it is

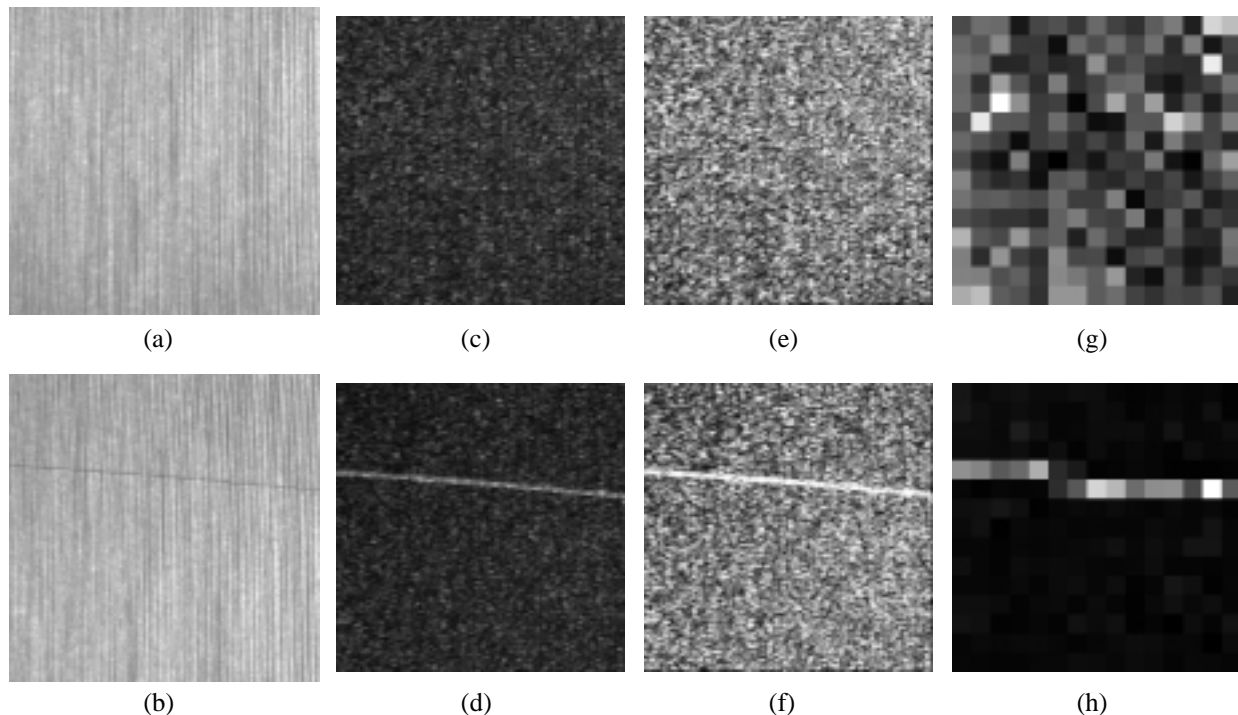


Fig. 7. (a), (b) Images of fabric without and with a defect, respectively. (c)-(h) Outputs of the various modules in the segmentation algorithm. See text for details.

equipped with a novel defect segmentation technique, which was thoroughly tested under realistic conditions and was found to have a high detection rate and accuracy and a low rate of false alarms. The fabric inspection system was described in terms of its image acquisition subsystem and its defect segmentation algorithm. The image acquisition subsystem is used to capture high-resolution, vibration-free images of the fabric under construction. The essence of the presented segmentation algorithm is the localization of those defects in the input images that disrupt the global homogeneity of the background texture. To accomplish this, a wavelet-based prepro-

cessing module, followed by an image fusion scheme, are employed to attenuate the background texture and accentuate the defects. Novel texture features are utilized to measure the global homogeneity of the output images. A prototype system was used to acquire and to analyze more than 3700 images of fabrics that were constructed with two different types of yarn. In each case, the performance of the system was evaluated as an operator introduced defects from 26 categories into the weaving process. The overall detection rate of the presented approach was found to be 89% with a localization accuracy of 0.2 in. and a false alarm rate of 2.5%.

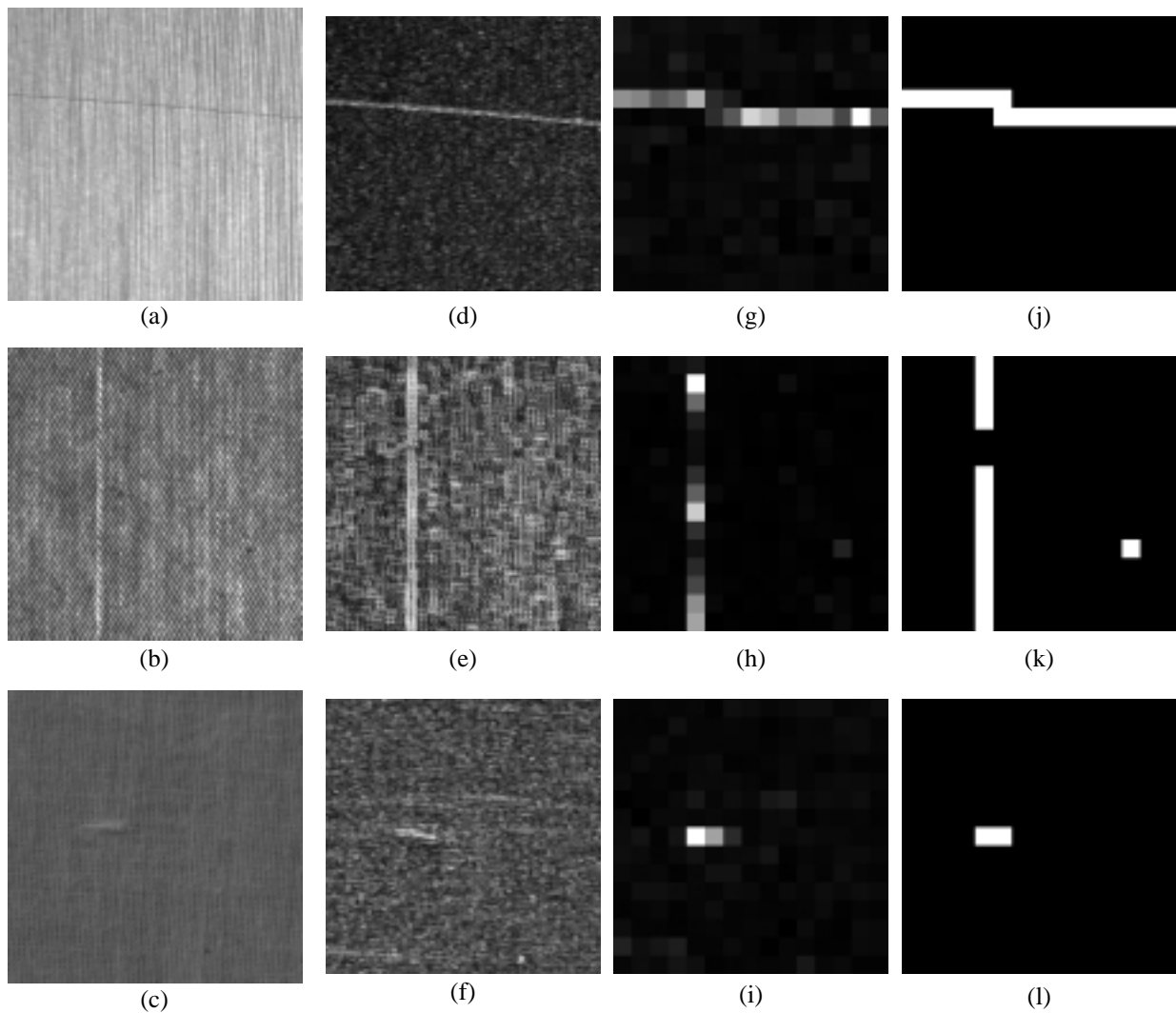


Fig. 8. (a), (b), (c) Fabric images with mispick, end-out, and slub (or waste) defects, respectively; with the corresponding fused outputs in (d), (e), and (f); $R(m, n)$'s in (g), (h), and (i); and the thresholded results in (j), (k), and (l).

REFERENCES

- [1] J. Huart and J. G. Postaire, "Integration of Computer Vision onto Weavers for Quality Control in the Textile Industry," *Proc. of SPIE Machine Vision Applications in Industrial Inspection II*, pp. 155-163, 1994.
- [2] B. W. Crowley, "Application of One-Dimensional Machine Vision in the Textile Industry," *IEEE Trans. on Industry Applications* **26**(2), pp. 324-329, March-April 1990.
- [3] J. Laitinen and I. Moring, "Method for Evaluation of Imaging in Automated Visual Web Inspection," *Optical Engineering* **36**(8), pp. 2184-2196, August 1997.
- [4] J. L. Dorrity, G. Vachtsevanos, and W. Jasper, "Real-Time Fabric Defect Detection and Control in Weaving Processes," *National Textile Center Annual Report*, pp. 113-122, November 1996.
- [5] S. Karkanis, C. Metaxaki-Kossionides, and B. Dimitriadis, "Machine-Vision Quality Inspection System for Textile Industries Supported by Parallel Multitransputer Architecture," *Microprocessing and Microprogramming* **28**(1), pp. 247-252, March 1990.
- [6] I. Erenyi and J. Pongracz, "Quality Control in Textile Industry via Machine Vision," *Microprocessing and Microprogramming* **32**(1), pp. 807-813, August 1991.
- [7] T. Thierry and M. Cattoen, "Automatic Inspection of Simply Patterned Material in the Textile Industry," *Proc. of SPIE Machine Vision Applications in Industrial Inspection II*, pp. 2-12, 1994.
- [8] F. S. Cohen, Z. Fan, and S. Attali, "Automated Inspection of Textile Fabrics Using Textural Models," *IEEE Trans. on Pattern Analysis and Machine Intelligence* **13**(8), pp. 803-808, August 1991.
- [9] K. Srinivasan, P. H. Dastoor, P. Radhakrishnaiah, and S. Jayaraman, "FDAS. A Knowledge-Based Framework for Analysis of Defects in Woven Textile Structures," *Journal of the Textile Institute* **83**(3), pp. 431-448, 1992.
- [10] S. Sardy and L. Ibrahim, "Experimental Medical and Industrial Applications of Neural Networks to Image Inspection using an Inexpensive Personal Computer," *Optical Engineering* **38**(8), pp. 2182-2187, August 1996.
- [11] L. M. Hoffer, F. Francini, B. Tiribilli, and G. Longobardi, "Neural Networks for the Optical Recognition of Defects in Cloth," *Optical Engineering* **35**(11), pp. 3183-3190, November 1996.
- [12] W. J. Jasper, S. J. Garnier, and H. Potlapalli, "Texture Characterization and Defect Detection Using Adaptive Wavelets," *Optical Engineering* **35**(11), pp. 3140-3149, November 1996.
- [13] H. Sari-Sarraf and D. Brzakovic, "A Shift Invariant Discrete Wavelet Transform," *IEEE Trans. on Signal Processing* **45**(10), pp. 2621-2626, October 1997.
- [14] S. G. Mallat, "A Theory for Multiresolution Signal Decomposition: The Wavelet Representation," *IEEE Trans. on Pattern Analysis and Machine Intelligence* **11**(7), pp. 674-693, July 1989.
- [15] I. Daubechies, "Orthogonal Bases of Compactly Supported Wavelets," *Comm. Pure and Appl. Math* **41**, pp. 909-996, 1988.
- [16] M. B. Abdulghafour, "Data Fusion Through Fuzzy Reasoning Applied to Feature Extraction from Multi-Sensory Images," pp. 189-190, Ph.D. Dissertation, The University of Tennessee, December 1992.
- [17] R. C. Gonzalez and R. E. Woods, *Digital Image Processing*, Addison-Wesley Publishing Company, New York, 1993.
- [18] D. Brzakovic and H. Sari-Sarraf, "Automated Inspection of Nonwoven Web Materials: A Case Study," *Proc. of SPIE's Symposium on Electronic Imaging*, San Jose, CA, February 1994.
- [19] P. Grassberger and I. Procaccia, "Characterization of Strange Attractors," *Phys. Rev. Letters* **50**(5), pp. 346-349, 1983.
- [20] N. Otsu, "A Threshold Selection Method from Gray-Level Histograms," *IEEE Trans. on Systems, Man, and Cybernetics* **9**, pp. 62-66, 1979.
- [21] J. Kittler and J. Illingworth, "On Thresholding Selection Using Clustering Criteria," *IEEE Trans. on Systems, Man, and Cybernetics* **15**, pp. 652-655, 1985.